

REPORT DOCUMENTATION PAGE			Form Approved OMB No 0704-0188	
Public reporting burden for this collection of information is estimated to average 1 hour per response, including the time for reviewing instructions, searching existing data sources, gathering and maintaining the data needed, and completing and reviewing the collection of information. Send comments regarding this burden estimate or any other aspect of this collection of information, including suggestions for reducing this burden, to Washington Headquarters Services, Directorate for Information Operations and Reports, 1215 Jefferson Davis Highway, Suite 1204, Arlington, VA 22202-4302, and to the Office of Management and Budget, Paperwork Reduction Project (0704-0188), Washington, DC 20503.				
1. AGENCY USE ONLY (Leave blank)	2. REPORT DATE	3. REPORT TYPE AND DATES COVERED FINAL REPORT 30 Sep 91 - 30 Sep 95		
4. TITLE AND SUBTITLE Surface Properties of Transition Metal Carbides		5. FUNDING NUMBERS 61102F 2301/ES AFOSR-TR- 96-0060		
6. AUTHOR(S) Dr Paul R. Davis		8. PERFORMING ORGANIZATION REPORT NUMBER		
7. PERFORMING ORGANIZATION NAME(S) AND ADDRESS(ES) Linfield Research Institute Linfield College 900 S. Baker Street McMinnville, OR 97128-6894		10. SPONSORING MONITORING AGENCY REPORT NUMBER AFOSR-91-0409		
9. SPONSORING/MONITORING AGENCY NAME(S) AND ADDRESS(ES) AFOSR/NE 110 Duncan Avenue Suite B115 Bolling AFB DC 20332-0001		11. SUPPLEMENTARY NOTES		
12a. DISTRIBUTION AVAILABILITY STATEMENT APPROVED FOR PUBLIC RELEASE: DISTRIBUTION UNLIMITED		12b. DISTRIBUTION CODE		
13. ABSTRACT (Maximum 200 words) Single crystal rods of ZrC and HfC were prepared by an arc float zone refinement technique. The electrical conductivities of ZrCx specimens have been measured at room temperature by a four-point probe method. Experiments were performed to study boron diffusion into ZrC specimens. The surface properties of ZrC single crystals were investigated, clean and with adsorbed oxygen and boron. The field emission characteristics of clean ZrC and HfC cathodes were measured. Evaporated films of ZrC showing carbide structure were grown successfully on polycrystalline Ta and W substrates and were characterized by Auger electron spectroscopy and X-ray photoelectron spectroscopy.				
14. SUBJECT TERMS		19960220 061		
17. SECURITY CLASSIFICATION OF REPORT UNCLASSIFIED		18. SECURITY CLASSIFICATION OF THIS PAGE UNCLASSIFIED		15. NUMBER OF PAGES
19. SECURITY CLASSIFICATION OF ABSTRACT UNCLASSIFIED		16. PRICE CODE		
20. LIMITATION OF ABSTRACT				

FINAL TECHNICAL REPORT
(9/30/91 - 9/30/95)

Report Date: 11/30/95

Title of Work: Surface Properties of Transition Metal Carbides

Grant No.: AFOSR-91-0409

Program Manager: Dr. Robert J. Barker
AFOSR/NE
Bolling AFB, DC 20332-6448

Contractor: Linfield Research Institute
Linfield College
900 S. Baker St.
McMinnville, OR 97128-6894

Contract Effective Date: 9/30/91

Contract Amount: \$497,243

Principal Investigator: Dr. Paul R. Davis
TEL: (503) 434-2524
FAX: (503) 434-2588
Internet: pdavis@linfield.edu

Co-Principal Investigator: Dr. William A. Mackie
TEL: (503) 434-2432
FAX: (503) 434-2588
Internet: billm@linfield.edu

Table of Contents

	Page
Summary	1
1. Background	2
2. Major Experimental Work Performed under this Contract.	2
2.1. ZrC Room Temperature Resistivity Measurements	2
2.1.1. Introduction	2
2.1.2. Experimental	3
2.1.3. Results.	4
2.1.4. Discussion.	5
2.2. Determination of Carbide Surface Properties	8
2.2.1. Introduction	8
2.2.2. Experimental	8
2.3. Diffusion of Boron into Macroscopic Single Crystal Carbide	13
2.4. Field Emission Properties of Single Crystals of Refractory Carbides	14
2.4.1. Introduction	14
2.4.2. High current density field emission	14
2.4.3. Close-spaced triode	18
2.4.4. Emission from rough emitter surfaces.	22
2.5. Emission Characteristics of Carbide Film Coated Field Emitters	24
2.5.1. Introduction	24
2.5.2. Experimental	24
2.5.3. Results and discussion	25
3. References	32
4. Publications and Presentations during the Program	34
4.1. Publications	34
4.2. Presentations	35

List of Figures

	Page
Figure 1. Schematic of four point probe resistivity experiment.	4
Figure 2. Resistivity versus composition for ZrC_x .	7
Figure 3. Thermionic effective work function of clean $ZrC_{0.92}(100)$.	9
Figure 4. Thermionic effective work function of clean $ZrC_{0.86}(100)$.	9
Figure 5. FERP work function of $ZrC_{0.92}(100)$ with adsorbed oxygen.	11
Figure 6. Thermionic effective work function of partially oxygen-covered $ZrC_{0.92}(100)$.	11
Figure 7. Thermionic effective work function of partially oxygen-covered $ZrC_{0.86}(100)$.	12
Figure 8. Thermionic effective work function of partially boron-covered $ZrC_{0.92}(100)$.	12
Figure 9. Depth profile of diffusion of B into ZrC single crystal.	13
Figure 10. Comparison of Fowler-Nordheim plots of emission from identically prepared emitters of ZrC, HfC and TaC.	15
Figure 11. Fowler-Nordheim slope vs intercept curves (constant β curves solid, constant ϕ curves dashed) showing data points of approach to high-current condition.	19
Figure 12. Schematic of the close-spaced triode structure.	20
Figure 13. Total emitted current vs position of emitter in close-spaced structure.	21
Figure 14. Variation of collector current with grid voltage in close-spaced field emission triode.	22
Figure 15. I - V characteristics for Si single emitter, clean and with ZrC film.	26
Figure 16. I - V characteristics for Mo single emitter, clean and with ZrC film.	27
Figure 17. Plotting Fowler-Nordheim slopes versus intercepts generates families of curves for constant ϕ (dashed lines) and constant β (solid lines). Data points are superimposed from Si emitters before and after deposition of ZrC films.	29
Figure 18. Fowler-Nordheim slope versus intercept plots, as in Fig. 17. Data points are superimposed from Mo emitters before and after deposition of ZrC films.	30
Figure 19. I - V characteristics for SRI field emission array, clean and with ZrC film.	31

SURFACE PROPERTIES OF TRANSITION METAL CARBIDES

Summary

Single crystal rods of ZrC and HfC were prepared by an arc float zone refinement technique. Single crystal specimens of compositions $\text{ZrC}_{0.92 \pm 0.04}$, $\text{ZrC}_{0.86 \pm 0.04}$ and $\text{ZrC}_{0.82 \pm 0.04}$ were fabricated for conductivity measurements and for surface studies.

The electrical conductivities of ZrC_x specimens have been measured at room temperature by a four-point probe method. The variation of resistivity with composition is discussed.

Experiments were performed to study boron diffusion into ZrC specimens. Diffusion specimens and controls were analyzed by cold neutron depth profiling at the NIST cold neutron facility in Gaithersburg, MD, and by Auger depth profiling in our laboratory.

The surface properties of ZrC single crystals were investigated, clean and with adsorbed oxygen and boron. Auger electron spectroscopy was used to determine surface compositions and field emission retarding potential and thermionic diode methods were used to measure work functions.

The field emission characteristics of clean ZrC and HfC cathodes were measured. High current density emission, greater than $1 \times 10^8 \text{ A/cm}^2$, was observed and is discussed. A method for determining the cathode changes leading to this high current emission condition is proposed. A close-spaced triode designed for testing individual emitters is described, and results are reported. The effective thermionic work functions of clean and partially oxygen covered surfaces of ZrC specimens of two different bulk compositions are reported and discussed. Clean values of 3.5 eV and 3.4 eV were observed for $\text{ZrC}_{0.92}$ and $\text{ZrC}_{0.86}$ specimens, respectively, at 1500K. With adsorbed oxygen, values as low as 3.4 eV and 3.2 eV, respectively, were observed for these surfaces at 1500K.

Evaporated films of ZrC showing carbide structure were grown successfully on polycrystalline Ta and W substrates and were characterized by Auger electron spectroscopy and X-ray photoelectron spectroscopy. ZrC films were deposited onto individual prefabricated Mo, Si and W field emitters, and demonstrated the capability for significant improvements in field emission characteristics. Films have also been deposited onto FEAs, demonstrating improvement in the FEA performance. These results are discussed.

SURFACE PROPERTIES OF TRANSITION METAL CARBIDES

1. BACKGROUND

The requirement, under the Vacuum Electronics Initiative, for pre-bunched emission of electrons at high current density has stimulated a substantial amount of research in development of arrays of field emission cathodes. The IVB transition metal carbides TiC, ZrC and HfC exhibit properties which make them potentially useful as field emission cathode materials. These carbides have work functions of the order of 3.5 eV, approximately 1 eV lower than the commonly used field emission cathode material tungsten. They have excellent electrical conductivities and are also very stable, with high melting points and resistance to chemical attack. They exist in the same crystal structure over a range of compositions ($0.8 < x < 1.0$ for ZrC_x , for example). We have been concentrating our research efforts on ZrC in this program, with some work on HfC as well, and we report on those efforts.

Zone refined single crystal rods of ZrC were prepared by a seeded arc float zone refinement growth technique, using seed crystals with desired orientations which were checked by Laué X-ray backscattering. The arc float zone refinement technique used to prepare these single crystal rods has been described in detail elsewhere.¹ Fundamentally, the technique involved forming a self-supporting droplet of the carbide, by means of an electrical arc struck between a counter electrode and a rod of the sintered starting material, and moving the molten region along the rod of material, under approximately one atmosphere of inert gas. The solidified single crystal rod cooled from the molten zone was used to prepare samples for the experiments discussed in this section.

In this final report, we present the results of the experiments we performed during the program. The report is subdivided into sections, one for each of the primary experimental projects. Each section presents the rationale of the approach, the experimental method employed and results and discussion of the particular experiment.

2. MAJOR EXPERIMENTAL WORK PERFORMED UNDER THIS CONTRACT

2.1. ZrC Room Temperature Resistivity Measurements

2.1.1. Introduction

Zirconium carbide exists over a range of stoichiometries, and it may be important to know the composition of a ZrC specimen for any particular application. We expected that the resistivity of a sample would be related to its composition, so we measured the room

temperature resistivity of zone melted ZrC crystals with three different compositions to determine whether such resistivity measurements could be directly correlated with sample composition. The results showed that the resistivity increased as the carbon content decreased in ZrC crystals, suggesting that the resistivity may give us fundamental information on the stoichiometry of the material.

2.1.2. Experimental

The experimental set-up used in this study is shown in Fig. 1. It consisted of a four-point probe built in our laboratory, a Tektronix CPS250 power supply, two Hewlett-Packard 3468B multimeters (one for current measurement, the other for voltage), and a Stocker and Yale traveling microscope for measuring each crystal's radius and length. The uncertainties in current and voltage measurements were $\pm 0.5\%$ and $\pm 0.6\%$, respectively. The resolution of the microscope was $\pm 1.3 \times 10^{-4}$ cm. A typical sample used in this study had a radius of about 0.13 cm and a length of about 2 cm. The uncertainties in measuring the radius and the length of the crystals were $\pm 0.5\%$ and $\pm 0.6\%$, respectively. Therefore, the maximum total measurement uncertainty was about $\pm 2\%$. The set-up was first calibrated by using a polycrystalline tungsten sample whose dimensions were comparable to those of the ZrC crystal samples. The nominal resistivity of tungsten is $5.65 \mu\Omega\cdot\text{cm}$. at room temperature², while the value determined by using our set-up was $5.66 \pm 0.11 \mu\Omega\cdot\text{cm}$.

The ZrC single crystals used in this study were arc float-zone refined from sintered stock. The details of this process are discussed elsewhere¹. The composition, or carbon to zirconium ratio (C/Zr), of the zone-refined crystals depended on the number of zone passes made through the material (initial composition C/Zr = 1.0) during refinement. The sample compositions were determined by chemical analysis.³ It was previously found that average C/Zr value are $\text{ZrC}_{0.92 \pm 0.04}$ for one zone pass, $\text{ZrC}_{0.86 \pm 0.04}$ for two zone passes, and $\text{ZrC}_{0.82 \pm 0.04}$ for three zone passes.

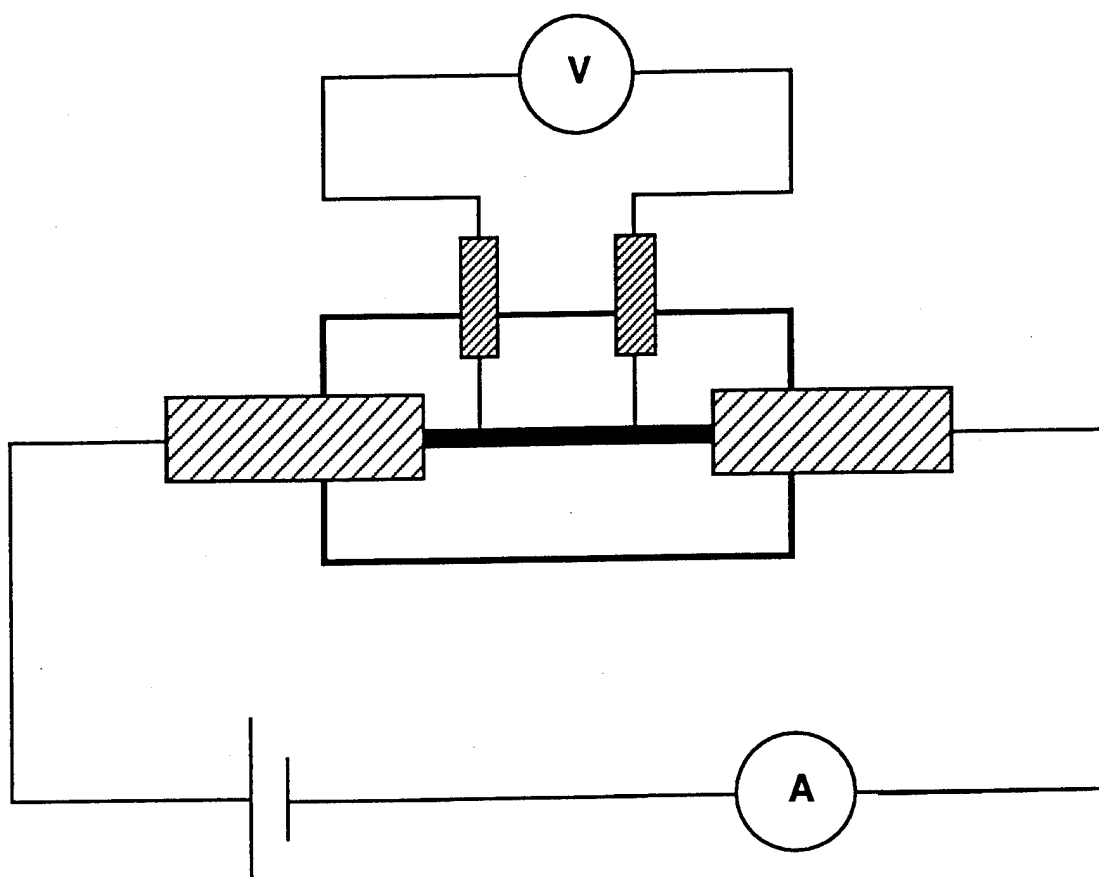


Figure 1. Schematic of four point probe resistivity experiment.

2.1.3. Results

The resistivities measured in this study for one, two, and three zone pass crystals are listed in Tables I, II, and III, respectively. In these measurements, different resistivity values for a particular crystal were observed by rotating the crystal. The range of resistivity for one-pass ZrC crystals was found to be $197.8 \leq \rho \leq 208.0 \mu\Omega\cdot\text{cm}$, and the mean value was $202.6 \pm 2.7 \mu\Omega\cdot\text{cm}$. The resistivity range for two-pass crystals was $202.5 < \rho < 228.7 \mu\Omega\cdot\text{cm}$, with a mean value was $214.6 \pm 7.7 \mu\Omega\cdot\text{cm}$. For three-pass crystals, $211.3 \leq \rho \leq 229.7 \mu\Omega\cdot\text{cm}$ with a mean value of $221.7 \pm 5.1 \mu\Omega\cdot\text{cm}$. These results compared favorably with results of other studies⁴⁻⁶. The standard deviation of the resistivity values for the same crystal resulted primarily from the rotation of the crystals between each measurement. This variation was lowest for one-pass crystals (up to $\pm 1.6\%$) and highest for two-pass crystals (up to $\pm 5.3\%$). For three-pass crystals the variation with rotation was as high as $\pm 2.3\%$.

Table I
Resistivities of One-Pass ZrC Crystals
($\mu\Omega\text{-cm}$)

Crystal Number	Measured Values						Mean	Stoichiometry C/ Zr	Standard Deviation
932	200.3	199.5	197.8	199.3	198.9	199.6	199.2	0.92 \pm 0.04	0.8
933	200.9	204.7	202.2	204.8	204.4	205.9	203.8	0.92 \pm 0.04	1.9
935	201.2	203.0	205.5	203.3	200.2		202.6	0.92 \pm 0.04	2.0
950	205.9	204.9	201.7	202.2	206.2		204.2	0.92 \pm 0.04	2.1
966	200.5	201.8	199.1	203.1	202.9		201.5	0.92 \pm 0.04	1.7
969	203.0	206.8	208.0	201.7	199.8	206.6	204.3	0.92 \pm 0.04	3.3
All One-Pass Samples							202.6	0.92 \pm 0.04	2.7

Table II
Resistivities of Two-Pass ZrC Crystals
($\mu\Omega\text{-cm}$)

Crystal Number	Measured Values					Mean	Stoichiometry C/ Zr	Standard Deviation
915	211.2	211.7	210.4	211.2	213.4	211.6	0.86 \pm 0.04	1.1
973	204.4	205.3	224.5	224.7	202.5	212.3	0.86 \pm 0.04	11.3
975	219.0	228.7	220.9	224.1	211.6	220.9	0.86 \pm 0.04	6.3
1003	223.5	207.9	206.9	217.0	214.0	213.9	0.86 \pm 0.04	6.8
All Two-Pass Samples						214.6	0.86 \pm 0.04	7.7

Table III
Resistivities of Three-Pass ZrC Crystals
($\mu\Omega\text{-cm}$)

Crystal Number	Measured Values					Mean	Stoichiometry C/ Zr	Standard Deviation
976	224.5	226.8	218.8	218.8	220.4	221.9	0.82 \pm 0.04	3.6
976*	213.5	221.5	221.0	221.3	211.3	217.7	0.82 \pm 0.04	4.9
993	223.5	229.7	219.9	228.5	225.6	225.4	0.82 \pm 0.04	3.9
All Three-Pass Samples						221.7	0.82 \pm 0.04	5.1

2.1.4. Discussion

Our results agree very well with previous work at comparable temperatures and on single crystal samples of composition similar to those we have used. Modine, *et. al.*⁶, determined the resistivity of $\text{ZrC}_{0.89}$ to be about 204 $\mu\Omega\text{-cm}$ at 300 K, while Allison *et. al.*⁵, reported a value of 195 $\mu\Omega\text{-cm}$ for $\text{ZrC}_{0.93}$ at 300 K. To our knowledge, no previous study of 300K resistivity vs composition comparable to our present work has been reported.

Although the resistivities of the ZrC single crystals of a given composition were found to vary by a substantial amount, the variation of resistivity as a function of composition was still significant. In the present work, the average resistivity increase between one pass ($\text{ZrC}_{0.92}$) and two pass ($\text{ZrC}_{0.86}$) crystals was 5.9%, while the average resistivity increase between one pass and three pass was 9.4%. Fig. 2 summarizes the results of our measurements. Although the standard deviation is substantial, there is an apparent linear dependence of the resistivity upon the C/Zr ratio or, in other words, on the carbon vacancy concentration.

Uncertainty in the resistivity measurements related to the rotation of the crystal was as high as $\pm 5.3\%$ for two-pass samples. The reasons for this variation are not well understood. A possible explanation could be defects or cracks in the crystal, or crystal grain boundaries if the specimen is not actually a single crystal. There is the possibility of stoichiometry variation within the crystal as well. The arc float zone refining technique which we use has a single counter electrode, melting the stock from one side, so there is the possibility of anisotropy in composition across the diameter of the specimen, which is averaged out by the chemical analysis method used to determine the composition. Other possible sources of variation could be from the measurement itself, such as variations in the degree of contact between the probes and the crystal, related to anisotropic surface contamination of the crystal, for example, the presence of oxidized areas on the crystal surface.

We have observed an increase in resistivity with an increase in the concentration of carbon vacancies in the ZrC. Since resistivity measurement on these crystals are relatively simple to make, this technique could provide a useful way to determine the stoichiometry of a crystal. In order for this technique to be useful, however, it will be necessary to reduce the crystal-to-crystal variations in the measurements and to determine what causes the variation in measured values when the crystals are rotated.

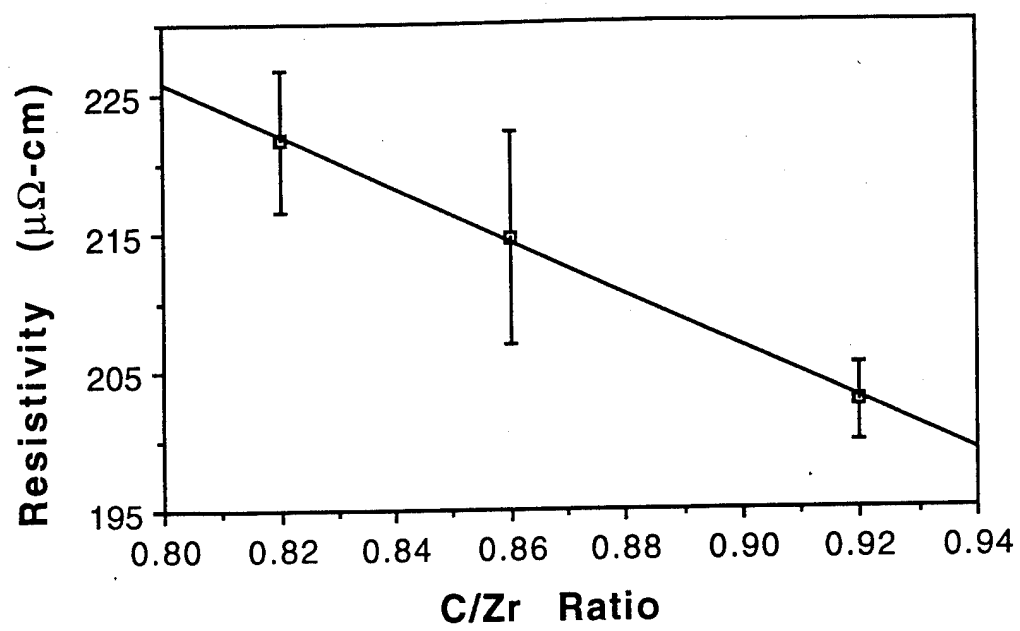


Figure 2. Resistivity versus composition for ZrC_x .

2.2. Determination of Carbide Surface Properties

2.2.1. Introduction

Specimens for surface studies using Auger electron spectroscopy (AES), X-ray photoelectron spectroscopy (XPS), and field emission retarding potential (FERP)⁷ work function measurements were prepared from single crystal rods of ZrC. Typically, it was useful to fabricate specimens with diameters of approximately 2 mm for these studies. The carbide rod was either cut by a diamond wheel or fractured to expose the desired surface. Only the (100) plane, which is the fracture plane of these materials, could be prepared by the latter technique. For many studies of the (100) surface, no additional polishing of the fracture surface was necessary. For studies of other crystal planes, it was necessary to mechanically polish the surface with diamond paste and electrochemically etch it before it was mounted.

The surface analysis specimen thus prepared was mounted by one of two techniques. One method was to cement the specimen into a thin Ta or Re cup using a Co/Ta braze, leaving the surface of interest exposed. The cup was spotwelded to a Ta wire which was mounted onto conducting supports, allowing the sample to be heated for cleaning and experimental studies. An alternative mounting method was to grind parallel flats onto the sides of the specimen and clamp it between pyrolytic graphite blocks, held in place by Mo/Re support rods. In this Vogel mount configuration, the specimen could also be heated.

2.2.2. Experimental

The surface properties of clean ZrC single crystals were investigated, using AES to determine surface composition and cleanliness and using FERP and thermionic diode methods to measure work functions. The surface and bulk compositions may differ substantially in crystals that have been heated. It is also possible that heating under the influence of a large applied electric field may cause changes in surface composition or structure which may affect the work function. We therefore performed studies of the differences in apparent surface compositions and differences in work functions between *in situ* fractured (unheated) specimen surfaces and heated or ion sputtered surfaces of specimens with known bulk composition. The work function of the (100) face of a previously heated single crystal specimen of bulk composition $\text{ZrC}_{0.92}$, measured by the FERP technique, has been determined to be about 3.6 eV. Thermionic effective work function measurements made on clean (100) surfaces of specimens with bulk compositions of $\text{ZrC}_{0.92}$ and $\text{ZrC}_{0.86}$ show lower values for $\text{ZrC}_{0.86}$ than for $\text{ZrC}_{0.92}$. These results are shown in Fig. 3 and Fig. 4.

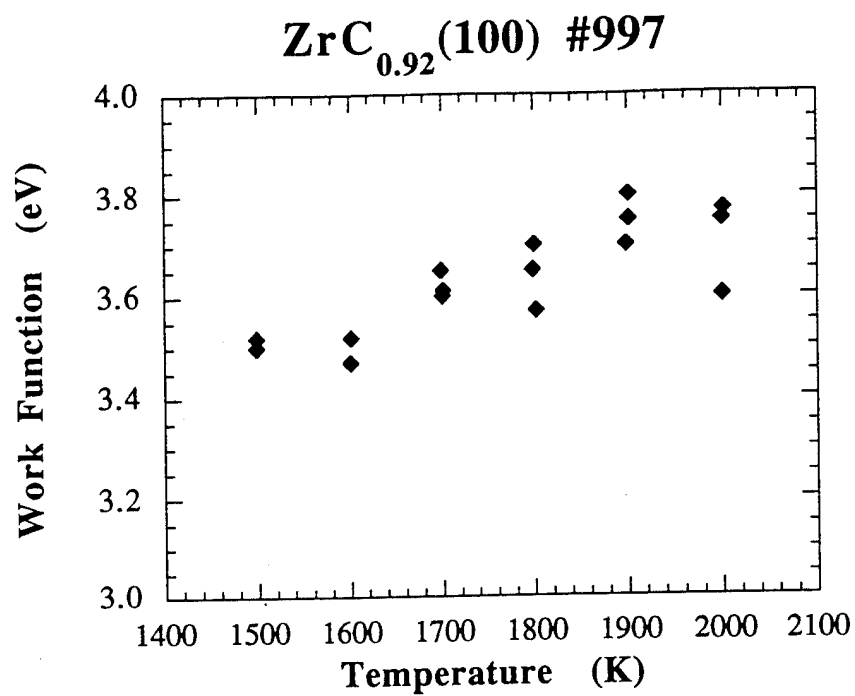


Figure 3. Thermionic effective work function of clean ZrC_{0.92}(100).

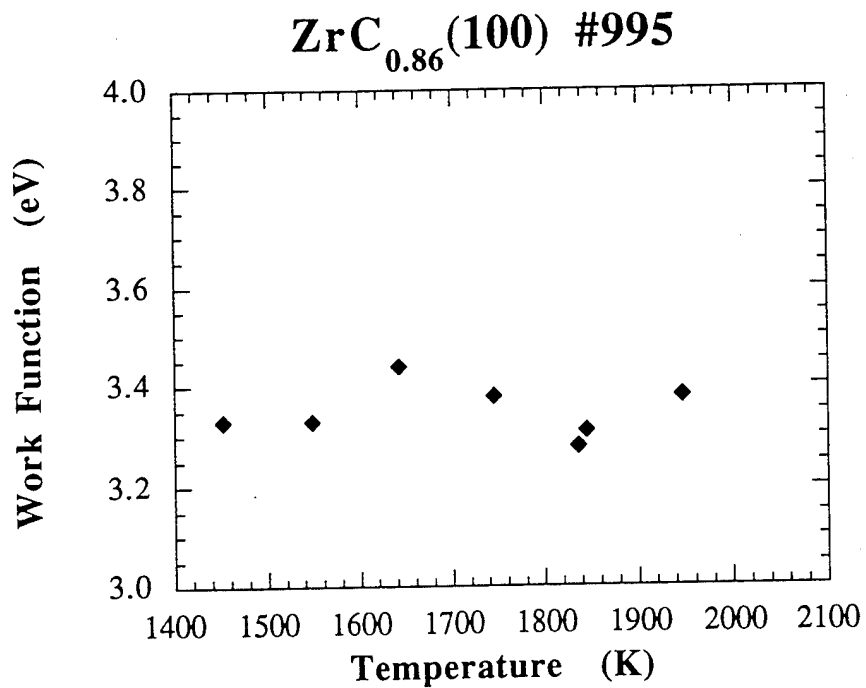


Figure 4. Thermionic effective work function of clean ZrC_{0.86}(100).

We also investigated the effects of adsorbed species on the work functions of single crystal ZrC surfaces. The effect of adsorption of oxygen at room temperature onto a ZrC surface is to raise the work function, as has been determined by room temperature FERP measurements. This behavior is shown in Fig. 5. However, adsorbed oxygen is difficult to remove by subsequent heating. Auger electron spectroscopy measurements following heating of adsorbed oxygen layers show that a small amount of residual oxygen remains on the surface. This apparently stable layer exhibits a lower thermionic work function than the corresponding clean surface. We believe that oxygen adsorption into surface carbon vacancies occurs, generating a surface layer with different properties from the clean ZrC surface. Oxygen atoms bonded in the surface or below surface atoms could produce a positive surface dipole layer, thereby accounting for the observed lower work functions. Figures 6 and 7 show the thermionic work function behavior for partially oxygen covered surfaces of (100) oriented specimens with bulk compositions of $\text{ZrC}_{0.92}$ and $\text{ZrC}_{0.86}$, respectively. At temperatures below about 1800K, Fig. 7 shows thermionic work functions which are lower with the residual oxygen present than for the clean surface. This effect is observed over the entire experimental temperature range in Fig. 6. The effect of oxygen on work function lowering, at low oxygen coverages, is more pronounced on the $\text{ZrC}_{0.86}$ specimen, the one with lower bulk carbon concentration and greater concentration of vacancies, supporting the speculation that oxygen interaction at surface vacancies or within the material lattice may be responsible for the work function lowering effect.

We also studied the effect of boron adsorption on surface properties of ZrC, using similar techniques. Boron, like oxygen, is an electronegative element and both oxycarbide and borocarbide compounds of Zr and Hf have been reported.⁸ However, boron is less electronegative than carbon, whereas oxygen is more electronegative. Figure 8 shows that the presence of any boron on a specimen with bulk composition $\text{ZrC}_{0.92}$ will raise the work function, regardless of the nature of subsequent treatment. Thus, there seems to be a fundamental difference between the incorporation of oxygen and the incorporation of boron into the surface or near-surface regions of ZrC.

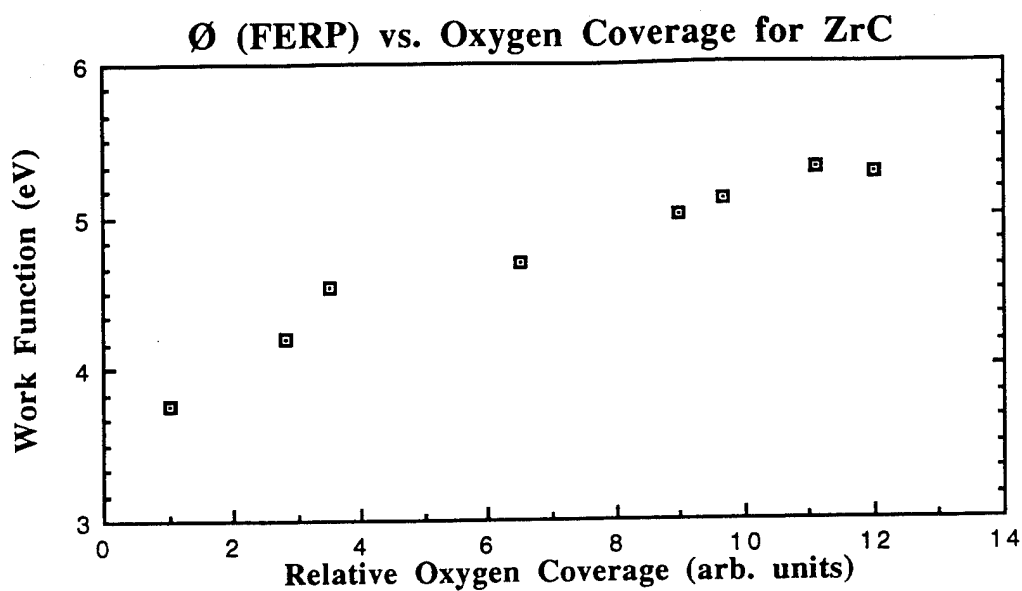


Figure 5. FERP work function of $\text{ZrC}_{0.92}(100)$ with adsorbed oxygen.

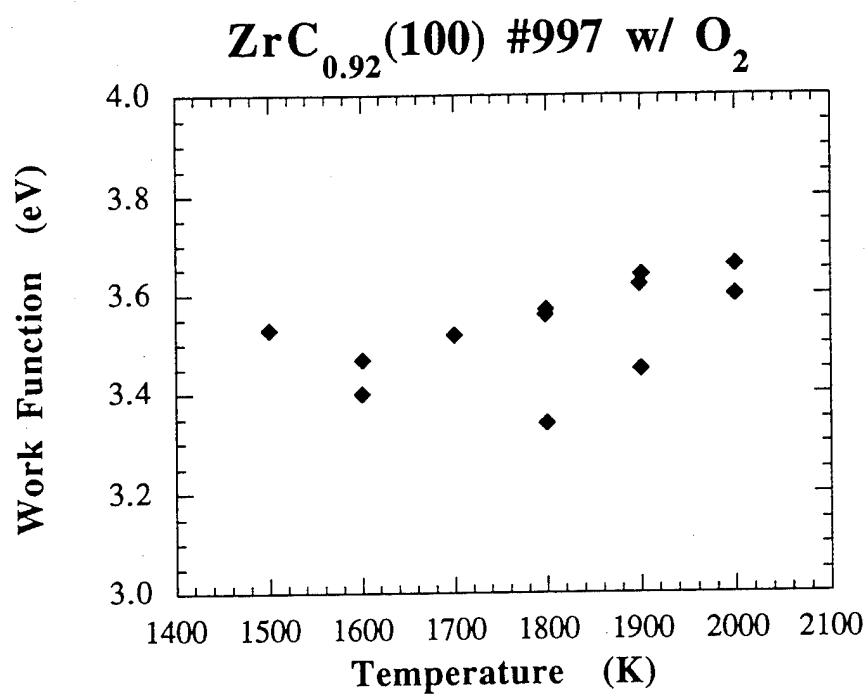


Figure 6. Thermionic effective work function of partially oxygen-covered $\text{ZrC}_{0.92}(100)$.

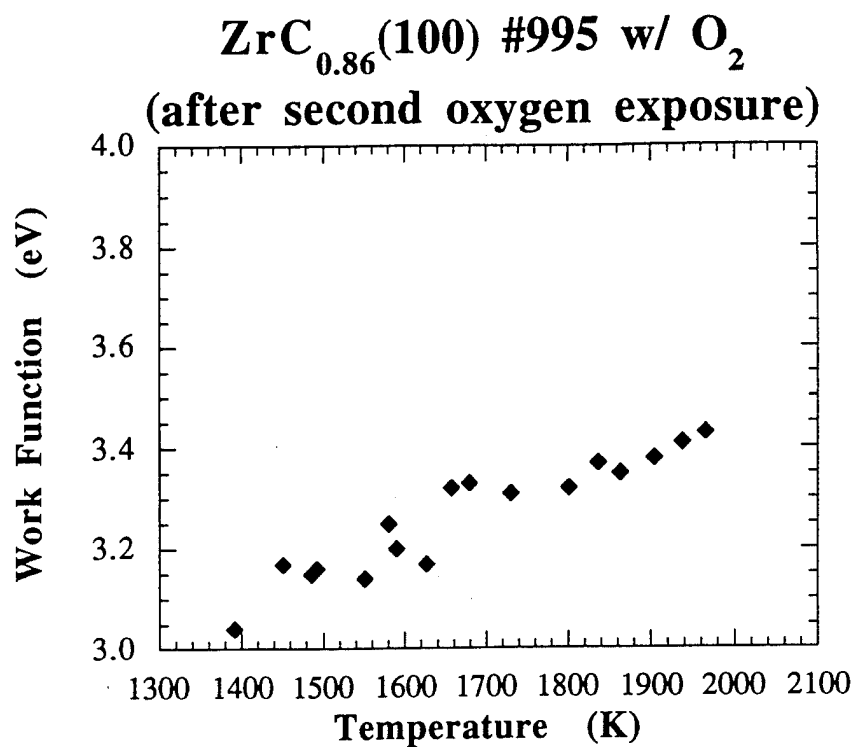


Figure 7. Thermionic effective work function of partially oxygen-covered ZrC_{0.86}(100).

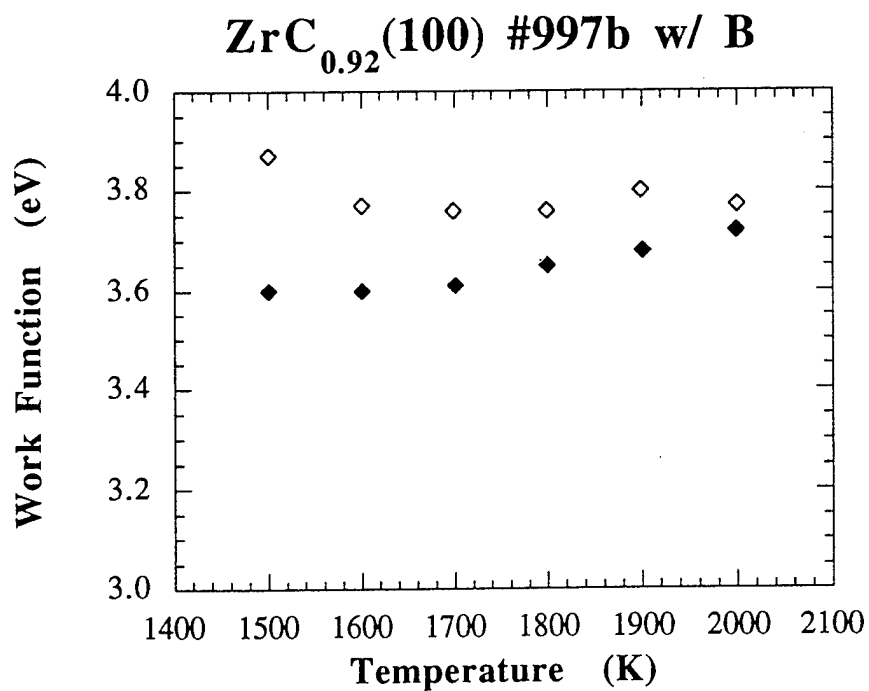


Figure 8. Thermionic effective work function of partially boron-covered ZrC_{0.92}(100).

2.3. Diffusion of Boron into Macroscopic Single Crystal Carbide

We investigated the diffusion of boron into ZrC and TiC specimens, in the following manner. A single crystal rod was packed with boron powder in a boron-resistant oven, which could be heated to over 2000K. The oven was then heated in vacuum and held at a constant temperature for a measured period of time. After cooling, the specimen was removed and analyzed.

For diffusion depths the order of one μm , neutron depth profiling⁹ could be used to determine the depth profile of B in the specimen. ZrC is a suitable specimen for these studies, because of the low neutron cross section of Zr. These measurements were done by our collaborator Dr. Greg Downing at NIST. For diffusion depths substantially greater, the specimen could be fractured *in situ* in the scanning Auger microscope (SAM) and the B concentration measured across the fracture face. For this situation, TiC is better than ZrC, because of an overlap between B and Zr Auger peaks. We found that B diffusion is detectable over at least 100 μm into the bulk of $\text{TiC}_{0.96}$, when diffusion took place at about 1500°C specimen brightness temperature for a period of 3600 sec.

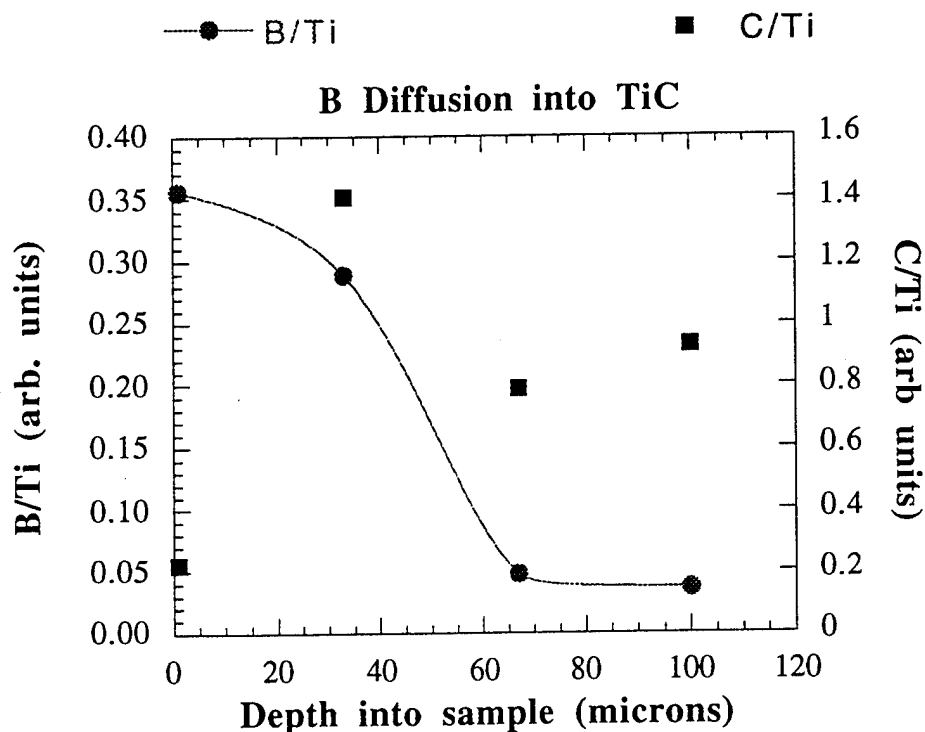


Figure 9. Depth profile of diffusion of B into ZrC single crystal.

2.4. Field Emission Properties of Single Crystals of Refractory Carbides

2.4.1. Introduction

The field emission characteristics of clean ZrC, HfC and TaC single crystal cathodes were studied. High current density emission, greater than 1×10^8 A/cm², was observed, and a method for determining the cathode changes leading to this high current emission condition was developed. A close-spaced triode designed for testing individual emitters was constructed and employed. The effective thermionic work functions of clean and partially oxygen covered surfaces of ZrC specimens of two different bulk compositions are reported and discussed. Clean values of 3.5 eV and 3.4 eV were observed for ZrC_{0.92} and ZrC_{0.86} specimens, respectively, at 1500K. With adsorbed oxygen, values as low as 3.4 eV and 3.2 eV, respectively, were observed for these surfaces at 1500K.

We have routinely prepared oriented, single crystal rods of these carbides by an arc float zone refinement technique discussed elsewhere.¹ These rods were then centerless ground, cut to length and electrochemically etched to make field emission cathodes.² The results of emission measurements on these cathodes are discussed in this section of the report.

2.4.2. High current density field emission

Figure 10 compares Fowler-Nordheim plots of field emission from ZrC_{0.92}, HfC_{0.86} and TaC_{0.74} cathodes, which were operated under essentially identical conditions in an ultrahigh vacuum field electron microscope. Data were taken after the emitters had been smoothed by heating and field desorption, yielding the characteristic smooth field emission pattern which was observed in each case. The patterns remained smooth during the experiments. Each emitter had its initial gross tip radius measured by SEM before being operated. Thus, it is possible to estimate the field enhancement factor, β , and the emitting area, so that the data may be presented in terms of the emitted current density, J , and the applied field, F . In principle, then, the slope in each case should be proportional to $\phi^{3/2}$. We have measured the clean work functions of macroscopic crystals of the same compositions and find for the (100) planes that $\phi_{\text{ZrC}} > \phi_{\text{TaC}} > \phi_{\text{HfC}}$. This is the same work function ordering implied by the relative slopes of Fig. 10.

Carbide F-N Comparison

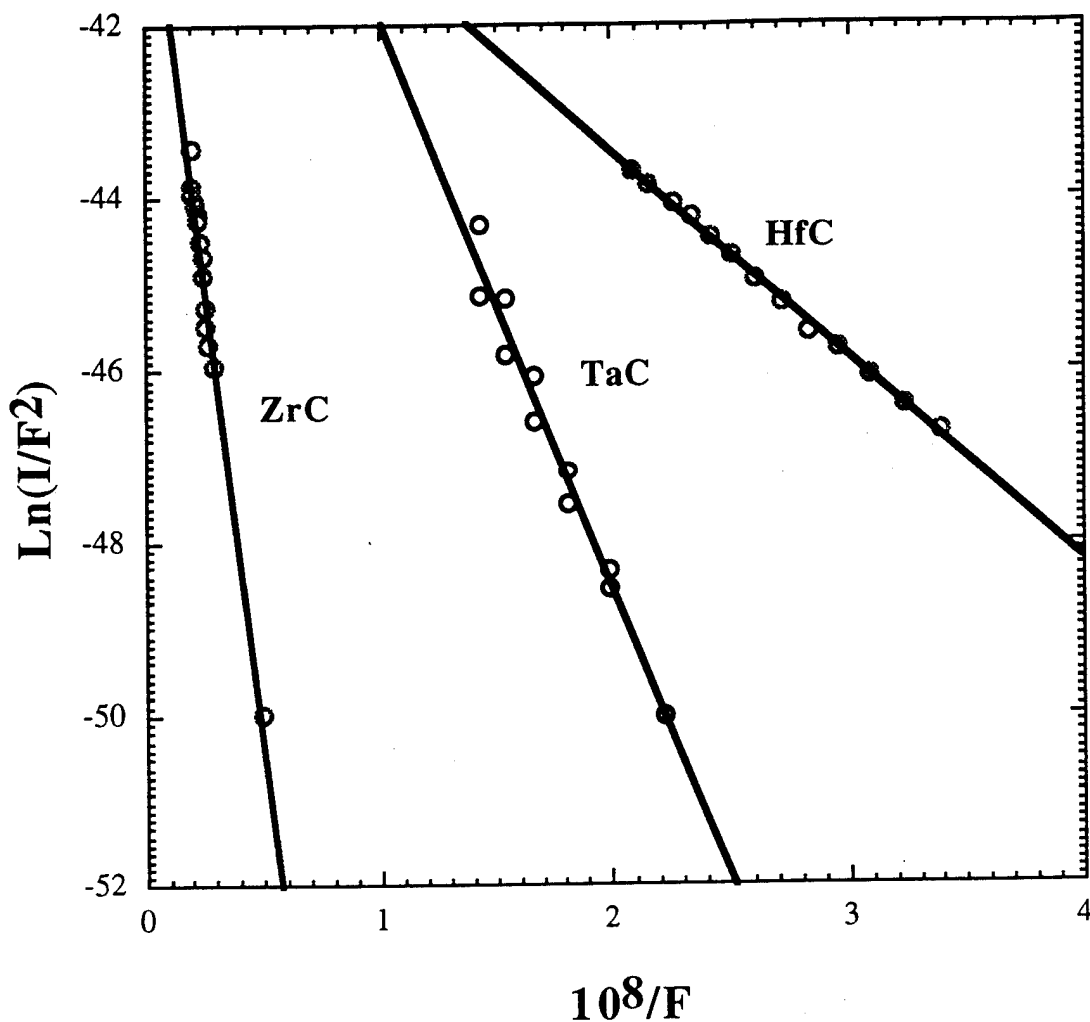


Figure 10. Comparison of Fowler-Nordheim plots of emission from identically prepared emitters of ZrC, HfC and TaC.

Table IV summarizes high current density field emission data which we have measured for HfC and ZrC emitters. The currents given in the second column are for pulsed operation (10 μ s pulse length) and correspond to the highest measured current for a particular condition of a particular emitter. The current density calculated in the last column is based on the initial tip radius, assuming an emission area equal to one half of a hemisphere of this radius. This rather conservative assumption still yields current densities of several times 10^8 A/cm² in many cases. A more realistic estimate of maximum current densities would be over twice the current densities listed. We have calculated, using a method described elsewhere¹¹, that the current density emitted at the apex of an ideally smooth,

homogeneous emitter is approximately twice the average emitted current over the entire emitter. In addition, the actual emission pattern is not homogeneous but exhibits high and low emission areas.

Table IV
High Current Density Field Emission
from Transition Metal Carbides

Hafnium Carbide				
emitter #	I (mA)	r (nm)	V (kV)	J (A/cm²)
677	9.4	180	10.0	9.2×10^6
"	10.3	"	10.0	1.0×10^6
91	12.0	31	6.4	4.0×10^8
"	9.8	"	5.8	3.3×10^8
"	5.4	"	5.2	1.8×10^8
52	18.3	70	5.0	1.2×10^8
785	7.5	125	8.32	1.5×10^7
Zirconium Carbide				
	10.6	50	10.0	1.2×10^8
	48.7	"	12.0	6.2×10^8

Stable DC field emission currents of 3 mA have been observed from some individual field emission cathodes, in addition to the high pulsed current levels shown in Table IV. There is a substantial change in cathode emission *I-V* characteristics which occurs before a cathode can achieve these high current levels. It has been unclear whether this change in *I-V* characteristics is due to work function decrease, change in emitter apex shape, or a combination of both. Once a cathode has achieved this high current condition, its emission stabilizes again at the high level and can remain there for an indefinite period. Furthermore, the high current condition can be achieved either by application of high DC fields with the cathode intentionally heated to at least 1500K, or by application of very high pulsed fields with no cathode heating.

In order to understand the mechanism responsible for the enhanced emission observed from some emitters, we have attempted to separate the variables ϕ (eV) and β (cm⁻¹) in the Fowler-Nordheim equation. The Fowler-Nordheim equation may be written as¹²

$$J = \{1.54 \times 10^{-6} F^2 / \phi t^2(y)\} \exp[-6.83 \times 10^7 \phi^{3/2} v(y) / F] \quad (1)$$

where $J = I/a$ (A-cm⁻²), the current per unit area of emitting surface, $F = \beta V$ (V-cm⁻¹), and

$$y = 3.79 \times 10^{-4} F^{1/2} / \phi. \quad (2)$$

As is appropriate for a paraboloid of revolution,¹² we assume

$$\beta = [0.5r \ln(D/r)]^{-1} \quad (3)$$

where r is tip radius and D is tip-to-anode spacing, and we make the approximations

$$t^2(y) = 1.05 \quad (4)$$

and

$$v(y) = 0.996 - y^2. \quad (5)$$

Therefore, when we make a Fowler-Nordheim plot of data we have

$$\ln(I/V^2) = \left[\ln(1.40 \times 10^{-6} a \beta^2 / \phi) + 9.81 \phi^{-1/2} \right] + \left[-6.60 \times 10^7 \phi^{3/2} / \beta \right] (1/V). \quad (6)$$

\uparrow
(INTERCEPT)

\uparrow
(SLOPE)

Thus, for any combination of ϕ and β we may extract the slope and intercept. Figure 11 shows a family of curves corresponding to constant ϕ and a family of curves corresponding to constant β . (This method is a slight modification of a technique described by Ishikawa, *et al.*¹³) These curves do not form an orthogonal set, since it is not strictly possible to separate these two parameters. Also shown in Fig. 11 are data points corresponding to the attainment of high current density I - V characteristics, during the application of very high applied pulsed fields. These data suggest that individual emitters achieve the high current density I - V characteristics by a process which involves maintenance of constant β , while the work function decreases. Data corresponding to low current density emission, before approaching the high current condition, do not seem to have this same trend.

The possibility that the highest current densities which we have observed are due primarily to reduction in work function is at least intuitively satisfying. When the emitters have made the transition from low emission to high emission, the behavior has almost always been self-stabilizing. That is, the emission has achieved a high level and stabilized without outside interference. If the tip were becoming sharper, it is difficult to understand why the process would stop, rather than continuing until the tip self destructed. It is more understandable that the work function decreases to some lower value, perhaps by field induced diffusion or some similar phenomenon within the surface region of the carbide, until a minimum work function is attained, at which point the changes stop. We have conducted measurements of the work functions of carbide surfaces, and the effects of contaminants on these surfaces, in a set of experiments described later in this report.

2.4.3. Close-spaced triode

A close-spaced triode structure (Fig. 12) was designed for testing individual carbide emitters. It incorporated a micrometer drive for axial positioning of the emitter apex within the replaceable grid aperture. An anode (collector) was placed about 1.5 mm downstream from the grid. The device was instrumented so that total emitted current, intercepted grid current, and collector current could be measured simultaneously.

The sensitivity of the triode to the precise axial emitter apex position has been explored, by carefully measuring the triode current at fixed applied DC voltages. Figure 13 shows the effect of axial tip position upon current measured at the collector. Note that the optimum collector current occurs when the tip of the emitter is flush with the collector side of the grid. The position corresponding to the maximum emitted current is approximately $z/t = 0.25$, but most of the current is intercepted by the grid at this position.

Figure 14 shows the behavior of electron emission from an emitter under a net applied voltage consisting of a DC bias plus an AC component. The experiment was set up in the following way. The emitter was held at ground potential, the collector was biased to 440 VDC, and the grid was biased at 450 VDC with an AC component of $\pm 1.5\%$ of the grid bias.

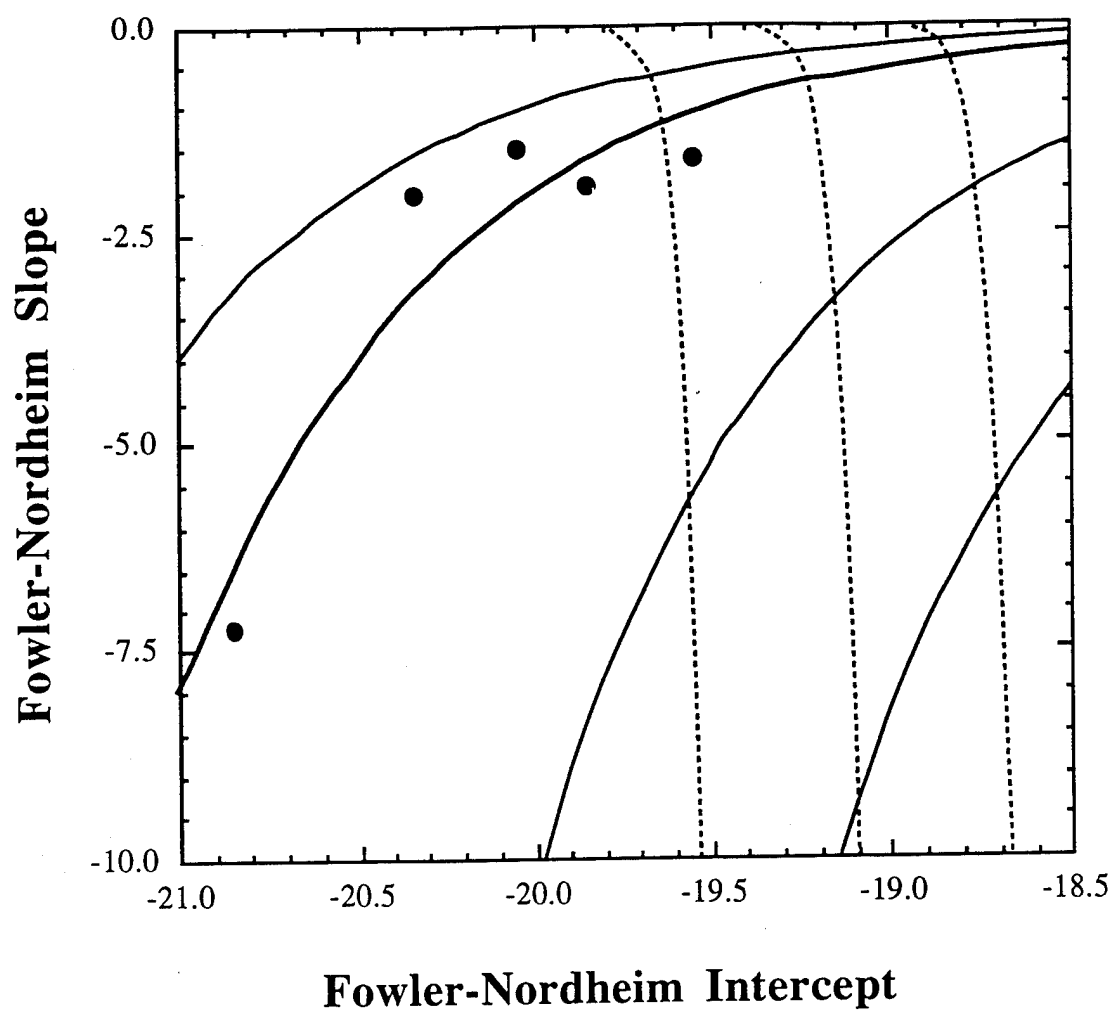


Figure 11. Fowler-Nordheim slope vs intercept curves (constant β curves solid, constant ϕ curves dashed) showing data points of approach to high-current condition.

Closed-Spaced Schematic

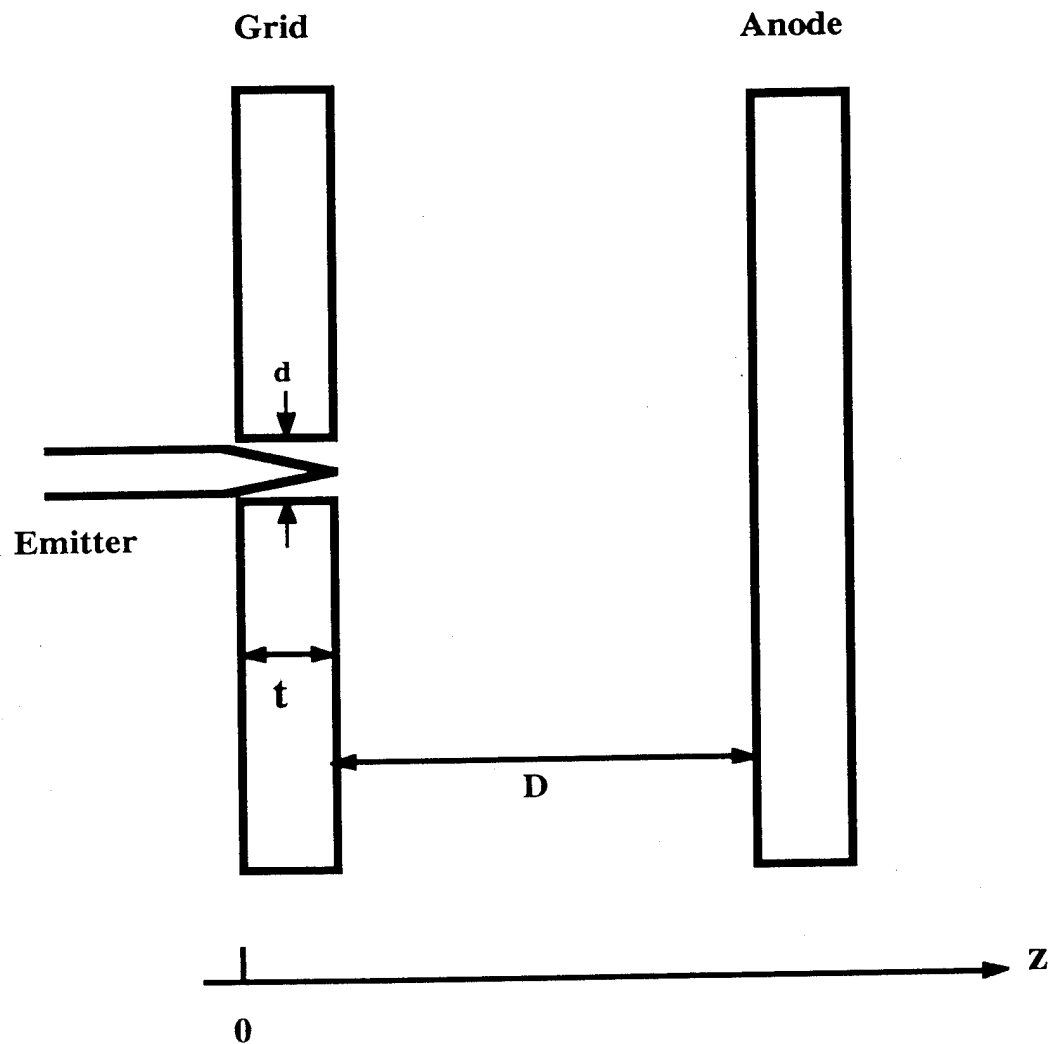


Figure 12. Schematic of the close-spaced triode structure.

Collected Current vs Tip Position

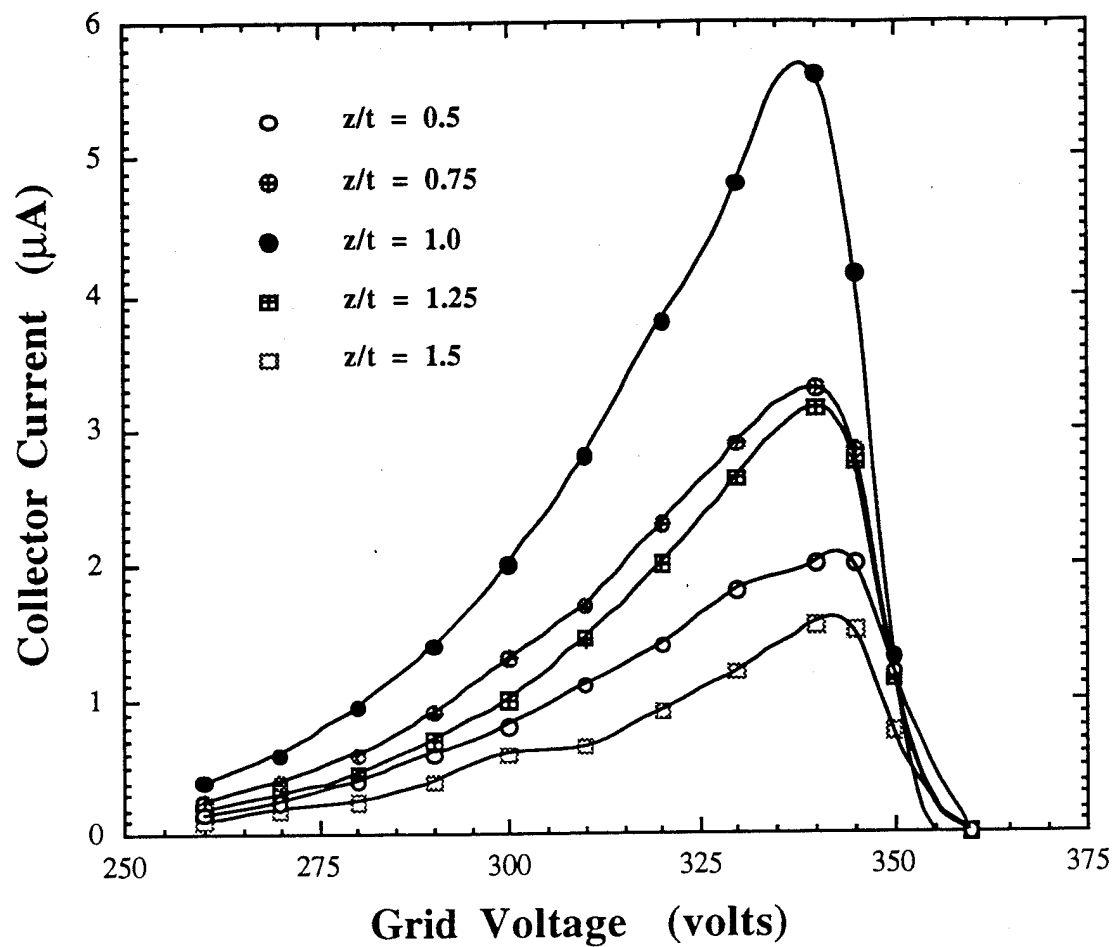


Figure 13. Total emitted current vs position of emitter in close-spaced structure.

Collector current response to 1.5% variation in grid voltage

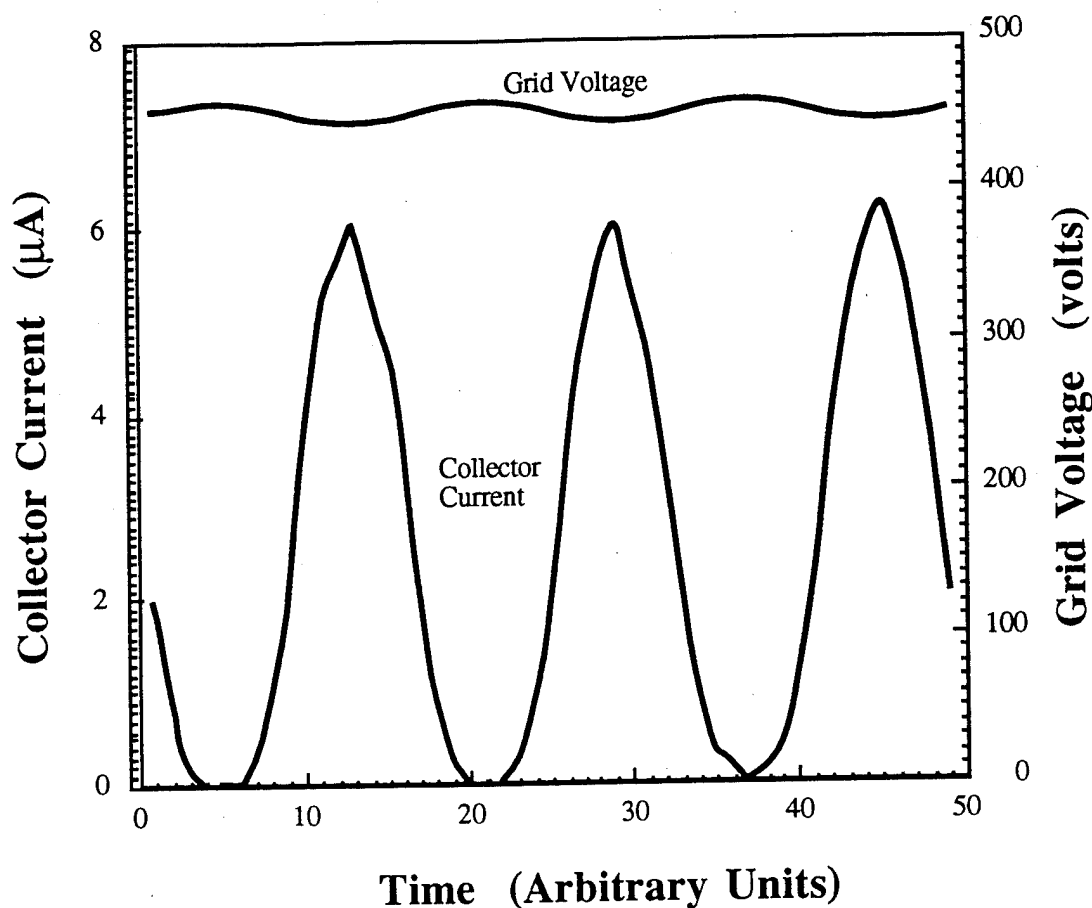


Figure 14. Variation of collector current with grid voltage in close-spaced field emission triode.

2.4.4. Emission from rough emitter surfaces

The field emission of electrons from surfaces is extremely sensitive to the local applied field, which is a strong function of the local radius of curvature. We have noted in our experiments the effect of surface roughness on total emission at a given applied voltage, for example observing that a rough emitter of 50 nm gross tip radius will emit more than a smooth emitter of 30 nm tip radius. Most of our experiments were performed in the FEM, where emission patterns can be observed. We exercised great care in these experiments to make sure that the emitter surface was smoothed, by a combination of heating and field evaporation, to produce a symmetric pattern free of emission from protrusions. In

experiments such as the close-spaced triode, and in fact in almost all practical applications, such careful tip preparation is not possible. Even SEM characterization of each emitter is not a solution, since we are unable to measure tip radii, and local roughness, with a resolution better than about 10 nm.

We have therefore modeled the effects of small local protrusions on the apex of an emitter of 50 nm radius, using a boundary element method already described. We used paraboloidal protrusions of radius 5 nm and heights 5, 10 and 15 nm, respectively. The results of these calculations are shown in Table V. The net effect in all cases is that virtually all the emission comes from the protrusion. That is, the local roughness of the emitter is more important than its gross tip radius, for emitters of the size we have investigated.

Table V
Calculated Effect of Single Paraboloidal Axial Protrusion
on Field Emission Current

Gross Tip Radius (nm)	Protrusion radius/height (nm/nm)	Current (amps)	Current Enhancement
50	0/0	4.75×10^{-9}	1
50	5/5	2.05×10^{-5}	4.3×10^3
50	5/10	1.69×10^{-4}	3.5×10^4
50	5/15	5.06×10^{-4}	1.1×10^5

2.5. Emission Characteristics of Carbide Film Coated Field Emitters

2.5.1. Introduction

Field emission from ZrC films deposited on Si and Mo single emitters and field emitter arrays (FEAs) made of Mo and Si has been studied. For single emitters, the results show dramatic improvements in emitter performance by reducing work functions on the order of 1 eV, and by increasing stability. For FEAs, deposition of a ZrC film reduced the operating voltage 30-50% at an emission current of 1.0 $\mu\text{A}/\text{tip}$ and increased emission stability.

We have shown^{14,15} that transition metal carbides such as ZrC and HfC have lower work function than materials such as Mo and Si which are used to make FEAs. In addition, compared to these materials, carbides have a higher resistance to contamination because of their chemical properties. That means field emission from carbide emitters will stay at the same level for a longer time. The successful FEAs, such as those made by SRI¹⁶ and MCNC¹⁷ are not made from carbides. The SRI cathodes are made from Mo, while the MCNC cathodes are made from Si. Both Mo and Si are relatively easier to form into tips than are carbides, and commercial Mo evaporators are available. Although we are also working on making carbide emitter arrays, this article is about coating Si and Mo single emitters and FEAs by ZrC. The goals were to achieve lower work function and a more stable emitting surface.

Our earlier work showed that ZrC films can be deposited epitaxially onto tungsten single crystals and onto single crystal emitters.^{14,18} A (100) ZrC film can grow on a W(100) surface while a (111) ZrC film can be formed on a W(110) surface, after careful annealing. The ZrC film lowers the work function by about 1 eV. Similar results were obtained on Mo emitters made from polycrystalline wires. For Si tips, things were more complicated. First, a single crystal emitter was hard to make by an electro-polishing method because the etching process is anisotropic. Second, a "clean" tip was not easy to obtain because of the low melting point of Si which limits the temperature used to heat-clean the tip. However, results showed a moderate work function decrease of 0.6 eV after ZrC was deposited.

2.5.2. Experimental

The single emitters used in this study were individually fabricated via electrochemical etching of polycrystalline wire (Mo) and single crystals (Si). The Mo emitters were etched in phosphoric acid and the Si emitters were etched in a solution of 5 parts concentrated HNO_3 and 1 part concentrated HF. Starting voltages were 10 volts for Mo and 25-35 volts

for Si, and drop off voltages were a few volts for Mo and ten volts for Si. Studies were also made on Mo FEAs obtained from SRI and on Si FEAs obtained from MCNC.

A high purity ZrC e-beam bombardment evaporation source was used to provide ZrC deposition. The ZrC used was a zone refined single crystal. Composition of the ZrC was checked by wet chemical analysis done in another lab as well as by Auger spectroscopy in our lab to ensure the purity of the ZrC crystal. Deposition coverage of ZrC was carefully studied by Auger spectroscopy using a Ta ribbon as a substrate.¹⁹ The calibration of film thickness was done by keeping the bombardment current and the high voltage fixed and varying the deposition time. By comparison of Zr and Ta peak heights in the Auger spectra, the time required for complete coverage of the substrate by the ZrC film was found. The results were used as a guide for later ZrC deposition onto field emitters and emitter arrays.

In practice, each single emitter was tested by a series run. In each run, the emitter was cleaned by heating up to about 2000 K (Mo) or 1300 K (Si) and field emission microscopy (FEM) was used to verify the crystal orientation and condition of the emitter apex. The idea here was to choose a temperature at which the emitters could be cleaned without being blunted too much. After a clean tip was obtained, an *I-V* data run (Figs. 15 and 16) was taken and was immediately followed by ZrC film deposition. Usually, the deposited ZrC film was a few monolayers thick. The film was then subjected to a variety of heating treatments. After each treatment, FEM was used to examine the tip and *I-V* data were obtained (Figs. 15 and 16). The observed lower "turn on" voltage for the dosed tip indicates that the work function of the dosed tip may be lower or the tip radius may be smaller, or both. Further investigations to study the nature of these changes were carried out by a technique developed earlier.¹¹ In this technique, the Fowler-Nordheim slope-intercept data of a tip before and after dosing were plotted onto a family of curves with constant work function and a family of curves of constant field enhancement factor (Figs. 17 and 18). The cause of lowering the "turn on" voltage could be inferred from this plot.

2.5.3. Results and discussion

The experimental results are listed in Table VI. We have successfully demonstrated the reduction of work function on W and Mo single crystal emitters. However, the results on a Si single tip were not quite as dramatic. This can be explained as follows. During the electrochemical polishing process to make the Si emitters, the tips were not isotropically etched. Very often the apex of the tip ended up with the shape of a knife edge instead of a

Silicon Single Emitter

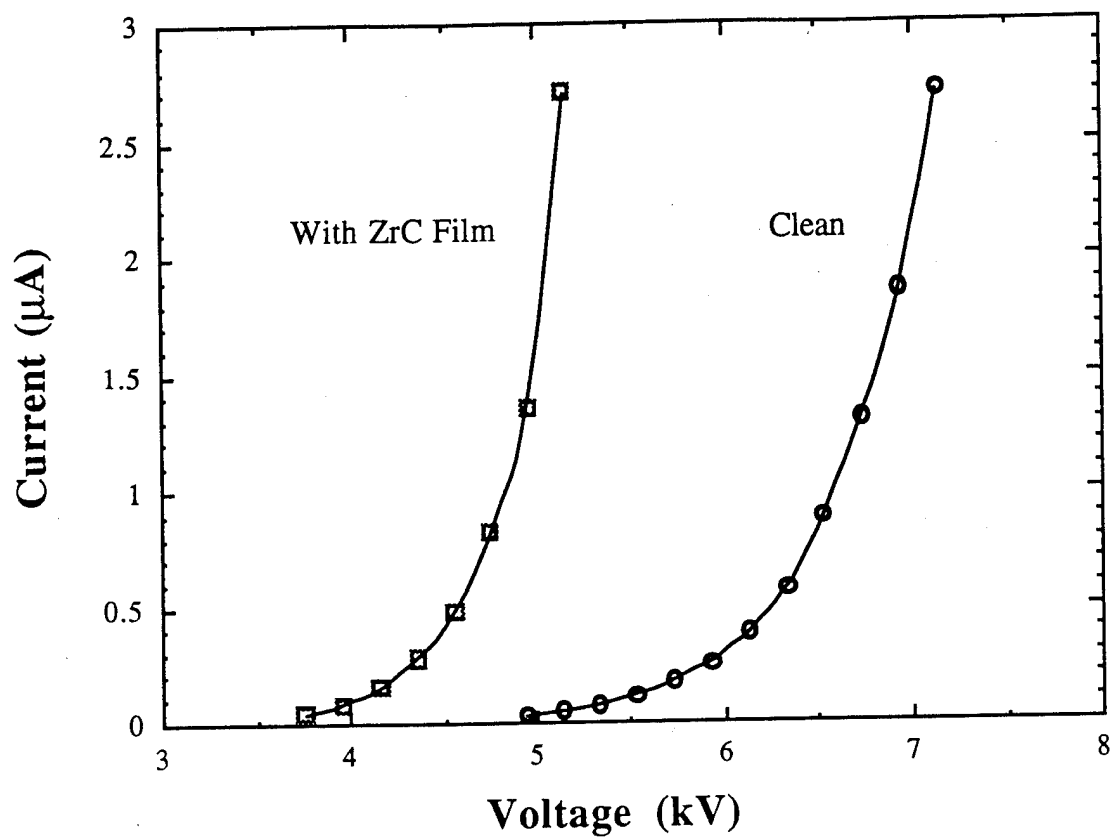


Figure 15. *I-V* characteristics for Si single emitter, clean and with ZrC film.

Molybdenum Single Emitter

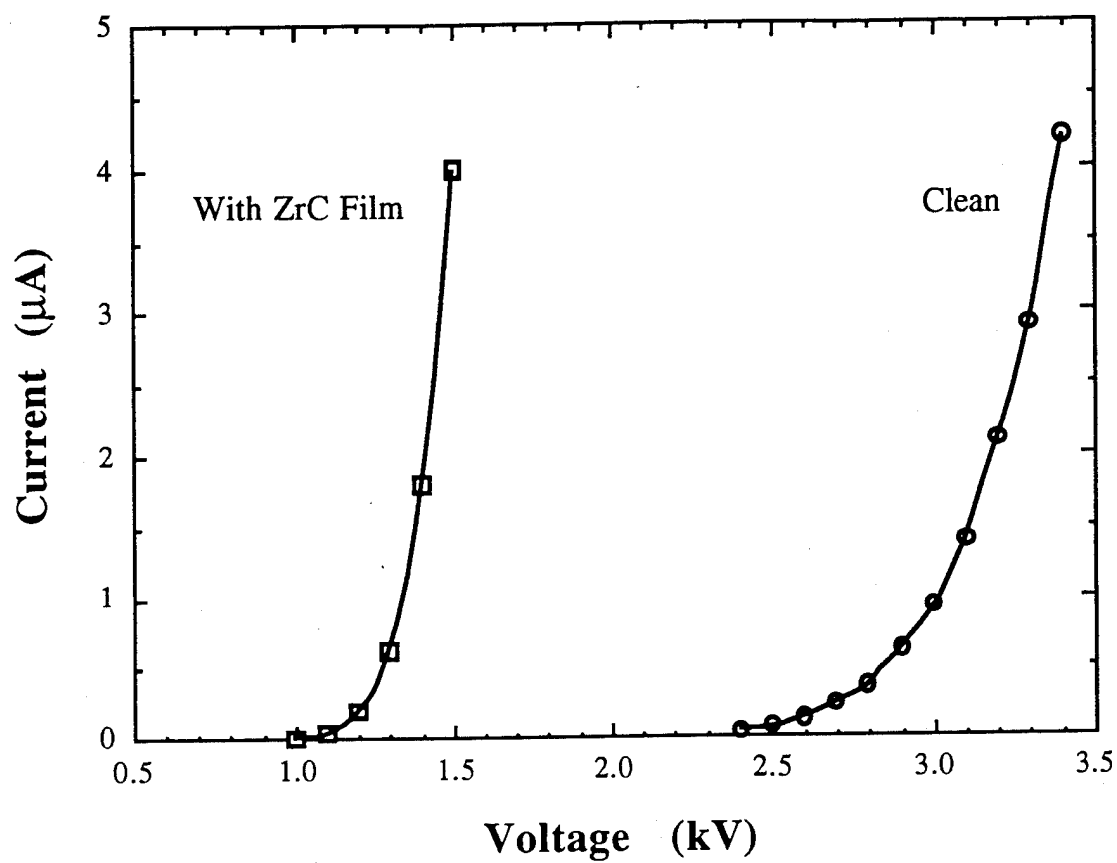


Figure 16. *I-V* characteristics for Mo single emitter, clean and with ZrC film.

sharp point. Therefore, the plane where the most field emission took place might not be the same before and after ZrC deposition. Furthermore, because of the low melting point of Si, the tips could not be heated enough to be free of contamination.

Our studies also show that the stability of the tips was improved. During the deposition of ZrC films, the work function was lowered and in most cases, the tip radius was increased. This can be seen from Fig. 17 and Fig. 18. Consequently, the work function lowering is responsible for the increased emission at lower turn-on voltages and the emission increase is not brought about by tip radius reductions.

Table VI
Results of Zirconium Carbide Film Deposition on Field Emitters

Substrate	Voltage Reduction @ same current	Work Function Ratio from F-N	Work Function Clean (eV)	Work Function with ZrC Film (eV)
W Single Emitter	38%	0.78	4.52	3.54
Mo Single Emitter	56%	0.64	4.60	2.95
Si Single Emitter	27%	0.87	4.82	4.19
Mo 100 Tip Array	44%	0.77	4.6	3.58
Si 1100 Tip Array	(23%)	(0.65)	4.85	3.15

Based on the success with individual tips, FEAs were able to be tested in a similar way. However, the FEA structures could be heated only to a few hundred degrees. Therefore, the tip cleaning procedure was simply to run the arrays at a reasonable current level (20-50 μ A) for a certain amount of time (two to three days for SRI FEAs). In the case of Spindt arrays, deposition of a ZrC film onto the emitters lowered the operating voltage by 30% to 50% at an emission current of 100 μ A. As with single tips, the effect was greater on Mo FEAs than on Si FEAs. A recent test showed that after a 149-hour run, a dosed Spindt FEA left to sit in the vacuum chamber for 10 days, still could be turned on again at the same output as before. Figure 19 shows a recent result on a SRI FEA. The results on FEAs are also listed in Table VI. The performance of ZrC dosed Si single emitters and MCNC FEAs was not as well studied as the W and Mo ones, and their performance characteristics are not as well known.

ZrC Film on Si Single Emitter

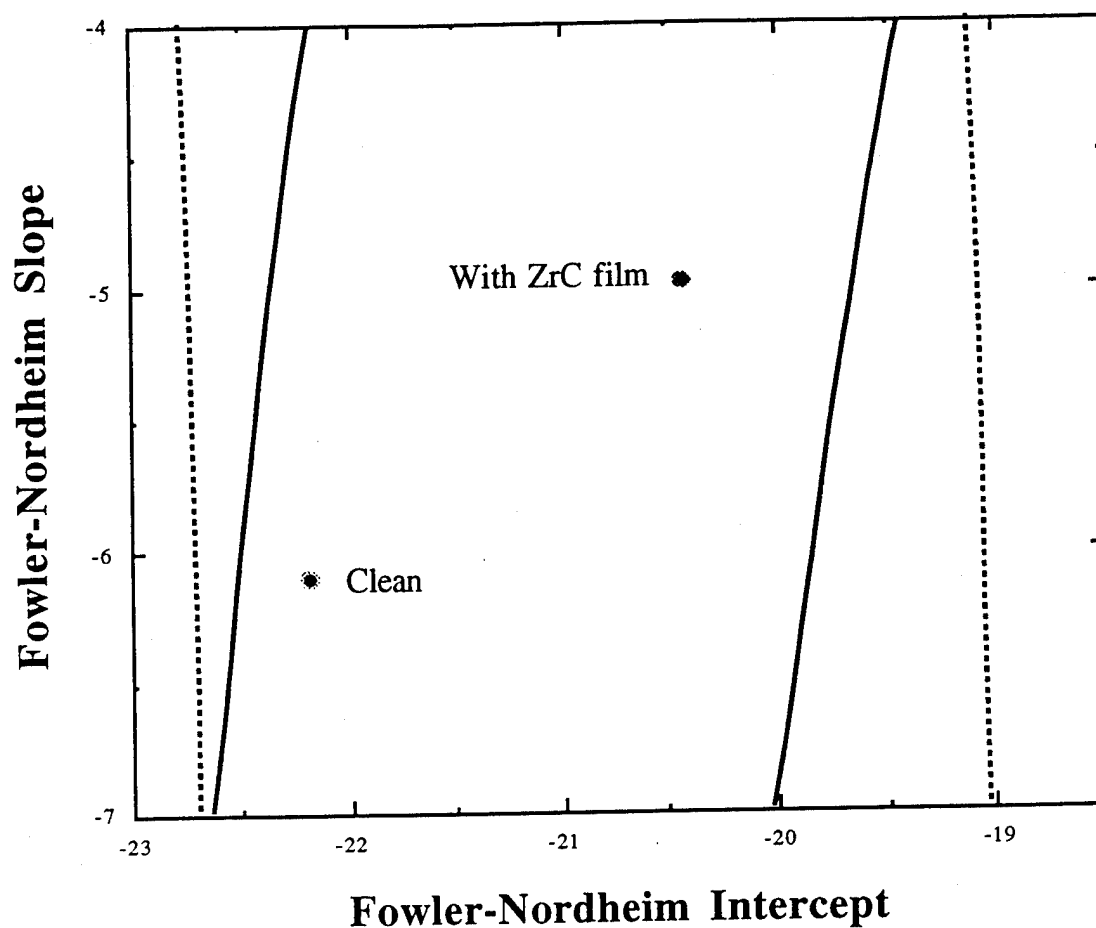


Figure 17. Plotting Fowler-Nordheim slopes versus intercepts generates families of curves for constant ϕ (dashed lines) and constant β (solid lines). Data points are superimposed from Si emitters before and after deposition of ZrC films.

ZrC Film on Mo Single Emitter

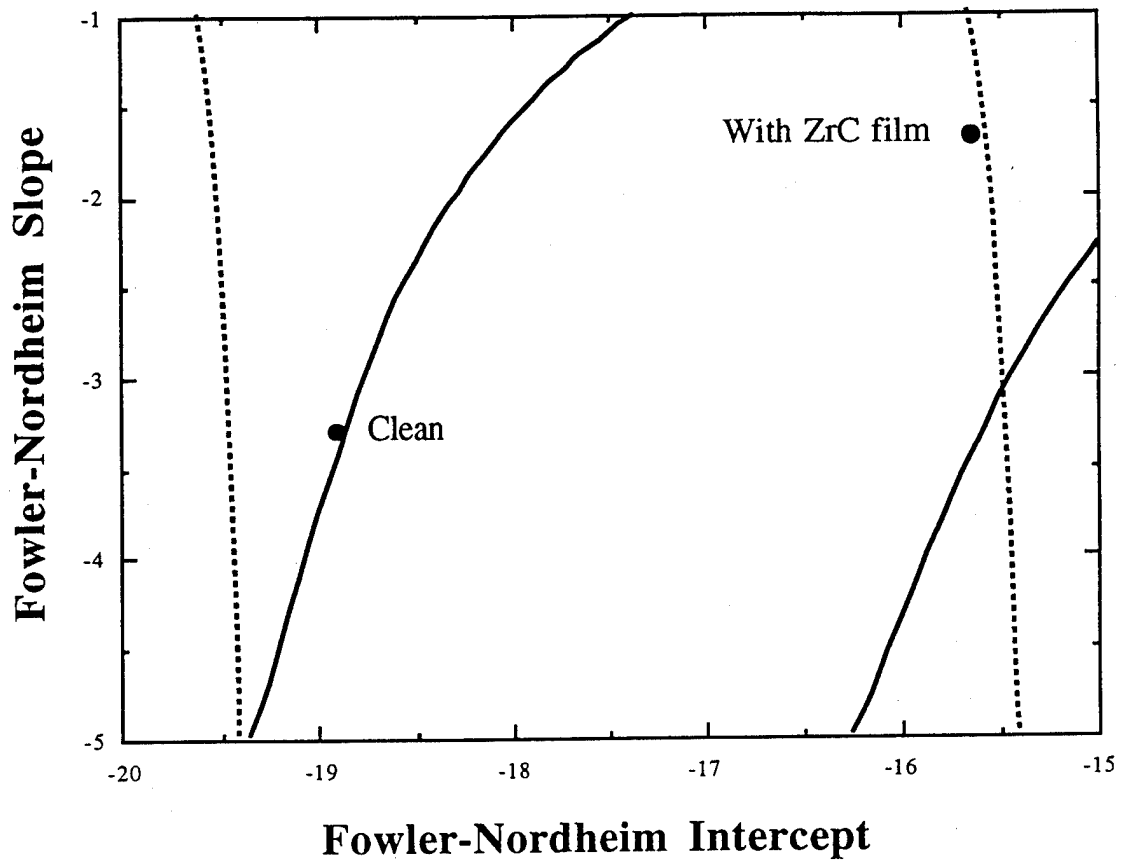


Figure 18. Fowler-Nordheim slope versus intercept plots, as in Fig. 17. Data points are superimposed from Mo emitters before and after deposition of ZrC films.

SRI Field Emitter Array

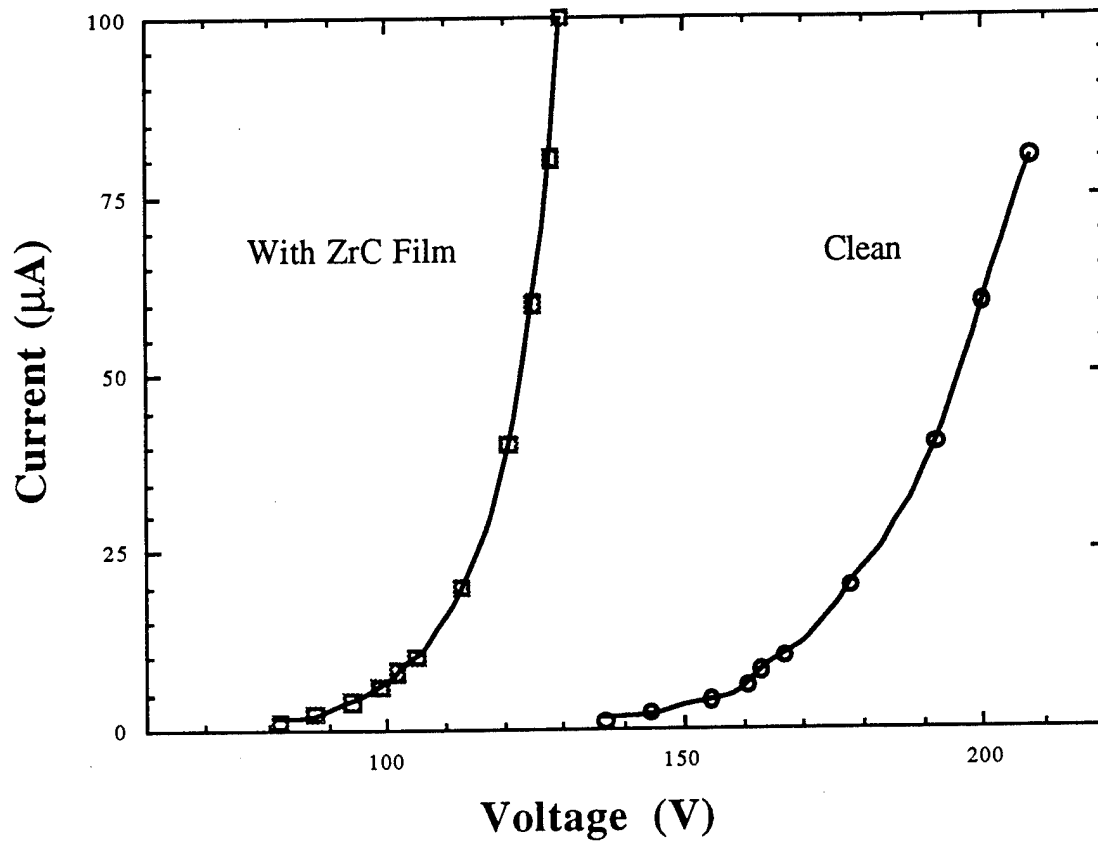


Figure 19. *I-V* characteristics for SRI field emission array, clean and with ZrC film.

3. REFERENCES

1. W. A. Mackie and C. H. Hinrichs, "Preparation of ZrCx Single Crystals by an Arc Melting Floating Zone Technique," *J. Crystal Growth* **87** (1988), 101.
2. *Handbook of Chemistry and Physics*, 60th Edition, R. C. Weast, ed., (CRC Press, Boca Raton, FL, 1979).
3. Measurements of composition were performed by Teledyne-Wah Chang Albany Analytical Labs by carbon combustion analysis and total weight measurement.
4. C. H. Hinrichs, M.H. Hinrichs, and W. A. Mackie, *J. Appl. Phys.* **68** (1990), 3401.
5. C. Y. Allison, C. B. Finch, M. D. Foegelle, and F. A. Modine, *Solid State Comm.* **68** (1988), 387.
6. F. A. Modine, T. W. Haywood, and C. Y. Allison, *Phys. Rev. B* **32** (1985), 7743.
7. R. W. Strayer, W. Mackie and L. W. Swanson, "Work Function Measurements by the Field Emission Retarding Potential Method," *Surf. Sci.* **34** (1973), 225.
8. E. K. Storms, *The Refractory Carbides* (Academic Press, New York, 1967).
9. R. G. Downing, R. F. Fleming, J. K. Langland and D. H. Vincent, "Neutron Depth Profiling at the National Bureau of Standards," *Nucl. Inst. Meth. Phys. Res.* **218** (1983), 47.
10. W. A. Mackie, R. L. Hartman and P. R. Davis, "High Current Density Field Emission from Transition Metal Carbides," *Appl. Surf. Sci.* **67** (1993), 29.
11. R. L. Hartman, W. A. Mackie, and P. R. Davis, "Use of Boundary Element Methods in Field Emission Computations," *IVMC 93* (Newport, RI, July 12-15, 1993)
12. R. Gomer, *Field Emission and Field Ionization*, (Harvard University Press, Cambridge, MA, 1961)
13. J. Ishikawa, H. Tsuji, Y. Gotoh, T. Sasaki, T. Kaneko, M. Nagao and K. Inoue, "Influence of Cathode Material on Emission Characteristics of Field Emitters for Microelectronic Devices," *J. Vac. Sci. Technol. B11* (1993), 403.
14. W. A. Mackie, Tianbao Xie, and P. R. Davis, "Field Emission from Carbide Film Cathodes," *J. Vac. Sci. Technol. B13* (1995), 2459.
15. W. A. Mackie, J. L. Morissey, C. H. Hinrichs, and P. R. Davis, "Field Emission from Hafnium Carbide", *J. Vac. Sci. Technol. A10* (1992), 2852.
16. Spindt-type field-emission array obtained from Capp Spindt, SRI International, Menlo Park, CA 94025.
17. Silicon tipped FEAs obtained from Chris Ball and Dev Palmer, MCNC, P.O. Box 12889, Research Triangle Park, NC 27709.

18. T. C. Tessner and P. R. Davis, "Preparation and characterization of crystalline ZrC films," *J. Vac. Sci. Technol. A* **11** (1993), 1.
19. W. A. Mackie, P. R. Davis and Tianbao Xie, "Field Emission from Carbide Film Cathodes," *Proc. 1994 Tri-Service/NASA Cathode Workshop*, ed. J. W. Gibson, (Palisades Institute for Research Services, Inc., Washington, DC, March 1994).

4. PUBLICATIONS AND PRESENTATIONS DURING THE PROGRAM

4.1. Publications

- P. R. Davis, W. A. Mackie and Tianbao Xie, "An Investigation of the Field Emission Characteristics of W, Mo and Si Emitters with Deposited ZrC Films," in 1995 Vacuum Electronics Annual Review (Palisades Institute for Research Services, Inc.).
- Tianbao Xie, W. A. Mackie, and P. R. Davis, "Field Emission from ZrC Films on Si and Mo Single Emitters and Emitter Arrays," (in press).
- W. A. Mackie, Tianbao Xie, and P. R. Davis, "Field Emission from Carbide Film Cathodes," *J. Vac. Sci. Technol. B* **13** (1995), 2459.
- W. A. Mackie, P. R. Davis and Tianbao Xie, "Field Emission from Carbide Film Cathodes," *Proc. 1994 Tri-Service/NASA Cathode Workshop*, ed. J. W. Gibson, (Palisades Institute for Research Services, Inc., Washington, DC, March 1994).
- R. L. Hartman, W. A. Mackie and P. R. Davis, "Use of Boundary Element Methods in Field Emission Computations," *J. Vac. Sci. Technol. B* **12** (1994), 754.
- W. A. Mackie, R. L. Hartman, M. A. Anderson and P. R. Davis, "Transition Metal Carbides for Use as Field Emission Cathodes," *J. Vac. Sci. Technol. B* **12** (1994), 722.
- W. A. Mackie, R. L. Hartman and P. R. Davis, "High Current Density Field Emission from Transition Metal Carbides," *Appl. Surf. Sci.* **67** (1993), 29.
- T. C. Tessner and P. R. Davis, "Preparation and Characterization of Crystalline ZrC Films," *J. Vac. Sci. Technol. A* **11** (1993), 1.
- W. A. Mackie, J. L. Morrissey, C. H. Hinrichs and P. R. Davis, "Field Emission from Hafnium Carbide," *J. Vac. Sci. Technol. A* **10** (1992), 2852.

4.2. Presentations

Tianbao Xie, W. A. Mackie, and P. R. Davis, "Field Emission from ZrC Films on Si and Mo Single Emitters and Emitter Arrays," International Vacuum Microelectronics Conference, Portland, OR, July 31-August 3, 1995.

P. R. Davis, W. A. Mackie and Tianbao Xie, "An Investigation of the Field Emission Characteristics of W, Mo and Si Emitters with Deposited ZrC Films, International Conference on Plasma Science, Madison, WI, June 5-8, 1995.

W. A. Mackie, Tianbao Xie and P. R. Davis, "Field Emission from Carbide Films Deposited on Prefabricated W and Mo Emitters," 1994 Microwave Power Tube Conference, Naval Postgraduate School, Monterey, CA, May 10-13, 1994.

P. R. Davis and W. A. Mackie, "Refractory Carbide Materials for Pulsed Field Emission Applications," 1992 Microwave Power Tube Conference, Monterey, CA, May 11-13, 1992.